The importance of e+A collisions at an Electron-Ion Collider

Matthew A. C. Lamont (BNL) for the EIC Science Task Force

Abstract: Over the last decade, there has been a plethora of new and exciting results in heavy-ion collisions emanating from the CERN and Brookhaven Laboratories. These results have led to a sea change of the view on how the evolution of a high energy heavy-ion collision proceeds. What has become apparent is that in order to validate claims of perfect fluidity, for example, the initial conditions at small-x need to be well understood. Whilst d+A and p+A collisions provide a handle on some of these effects, for precision measurements and precise knowledge of the kinematics, *e*+A collisions become essential.

A proposal has been developed at Brookhaven National Lab to add an electron accelerator to the current RHIC complex, providing for electron beams ranging from 5 GeV to 30 GeV. Complementing the programme on polarised e+p scattering, a broad programme on *e*+A physics is envisioned which will range from investigating saturation physics at low-x to hadronization at high-x. In this poster, I will show the recent progress made on the golden measurements which were identified in the proceedings of the Fall programme at the INT [1].

The eRHIC Accelerator Complex

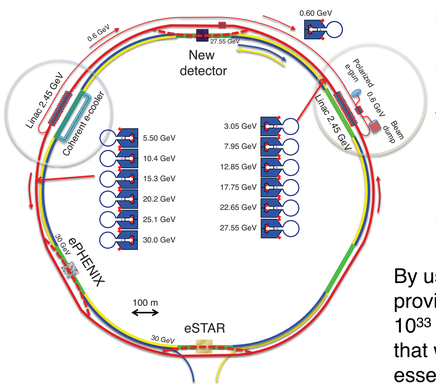

Figure 1: A schematic of the proposed eRHIC accelerator complex

In order to achieve the goals laid out in the abstract, a new electron-ion collider will need to be built. The most compelling design is to add an electron beam to the current RHIC complex, allowing for collisions in both present RHIC detectors and, importantly, in a new IP where a dedicated *e*+*p*(A) detector can be built using modern technologies and based upon the experiences gained from running at HERA.

By utilising an Energy Recovery LINAC (ERL) system as shown in Figure 1, it is envisioned that polarised electron energies from 5 GeV to 30 GeV can be reached, to go with the already achieved 100 (250) GeV for Au (protons).

By using an ERL, it will be possible to provide luminosities in the range of 10^{33}-10^{34} cm^{-2}s^{-1}, much higher than that which was achieved in HERA and essential for some of the physics programme

Figure 2 shows how the electron acceleration cavities fit nicely into the current RHIC tunnel. Note that in one pass around the eRHIC complex, the electron beam gains 5 GeV of energy. Therefore, to provide 30 GeV electron beams to the experiments, it is required that there are 6 beam passes through the RHIC tunnel.

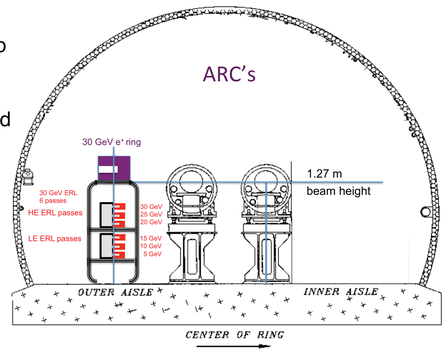

Figure 2: A schematic of how the e- beam fits into the RHIC tunnel

Deep-Inelastic Scattering

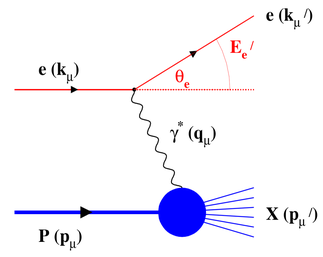

Figure 3: A schematic of a typical DIS event

$$Q^2 = 4E_eE_e'sin^2(\frac{\theta_e'}{2})$$ Measure of resolution power or "Virtuality"

$$y = \frac{pq}{pk} = 1 - \frac{E_{e'}}{E_e}cos^2(\frac{\theta_e'}{2})$$ Measure of inelasticity

$$x = \frac{Q^2}{2pq} = \frac{Q^2}{sy}$$ Measure of momentum fraction of struck quark

The best way to gain information on the structure of the nucleus is through Deep-Inelastic Scattering (DIS) as outlined in Figure 3. Here, a leptonic probe interacts with the nucleus via the exchange of a virtual photon (γ*). This process is much cleaner than *p*+A because which can be complicated by multiple colour interactions. The relevant kinematic quantities x, Q^2 and y - defined on the left - can also be exactly calculated in *e*+A collisions but this is not the case in *p*+A.

Figure 4 shows the x,Q^2 coverage of existing lepton+A measurements together with the coverage that will be achieved in *e*+A collisions at eRHIC. The red and black lines are for illustrative purposes and correspond to electron beam energies of 5 and 20 GeV respectively. It is readily noticeable that eRHIC will vastly extend the x,Q^2 coverage to lower x. As will be discussed in the next section and also presented in Figure 5, HERA discovered that this region in nucleons is dominated by sea quarks and in particular gluons [2]. In fact, gluons dominate the structure of the nucleon for x<10^{-1}. Whilst the sparse data for nuclei, illustrated in Figure 4, means that a similar plot is not available for nuclei, it is expected that the physics at eRHIC for both nucleons and nuclei will be dominated by gluons.

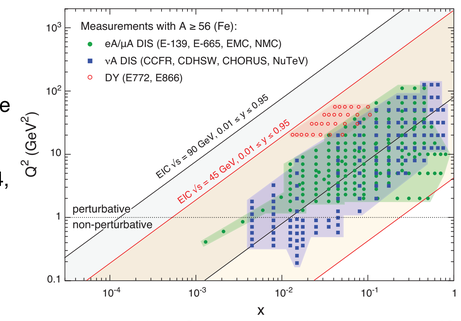

Figure 4: The x,Q^2 coverage of the proposed eRHIC

Saturation and the Nuclear Oomph Factor

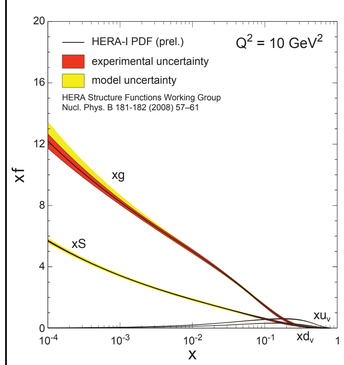

Figure 5: The partonic structure of the proton at Q^2=10 GeV^2

Figure 5 shows the result of a linear QCD (DGLAP) fit to *e*+*p* DIS data from HERA at Q^2 = 10 GeV^2, which represents the partonic structure of the nucleon as a function of x. What is surprising is the large gluon contribution at small-x. In fact, within the framework of linear QCD models, there is nothing to tame this explosive growth, coming from gluon splitting at low-x. Whilst the Froissart Unitarity Bound limits the cross section in hadron-hadron, interactions, this cannot be applied to *e*+*p* data. However, as the gluon density increases, it is believed that small-x gluons will recombine into higher-x gluons. These processes are described by the JIMWLK and BK non-linear QCD equations [3] and encapsulated in the Colour Glass Condensate (CGC) effective field theory [4].

When these gluon recombinations is equal or greater than the gluon splittings, it is said that saturation has occurred. The value in x,Q^2 where these are exactly equal and opposite is called the saturation scale, Q_s^2. This scale is outlined in Figure 6 where it is presented for protons, Ca and Au. Due to Lorentz contraction in the longitudinal direction of the accelerated ion, the Heisenberg Uncertainty Principle says that the small-x gluon will interact with the whole nucleus coherently. Geometric considerations show that the saturation scale in a nucleus is equal to that in a proton, multiplied by $A^{1/3}$. This leads to the curves in Figure 6, where Q_s^2 for Au is 6 times that in a proton. The energy coverage lines in Figure 6 show that at eRHIC, we should be able to probe well into the saturation regime. Also note that due to this effect, in a heavy nucleus like Au, we will effectively be probing values of x in the nucleon 2 orders of magnitude smaller than if we were to study *e*+*p* collisions at eRHIC. This has led to the coining of the phrase the nuclear "oomph" factor at eRHIC.

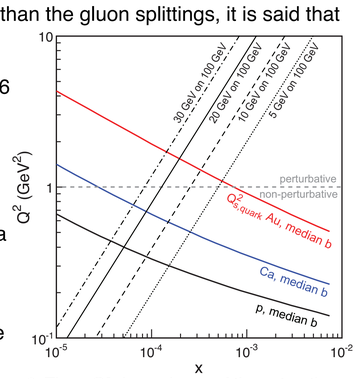

Figure 6: The x,Q^2 dependence of the saturation scale

Key Measurements 1: F_2 and F_L Structure Functions

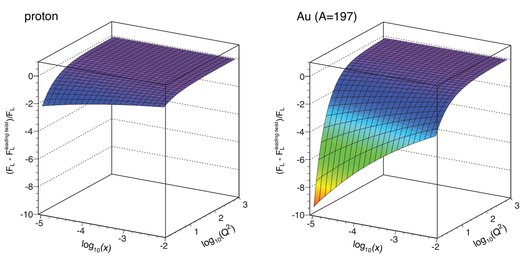

Figure 7: The contribution of higher order processes to F_L for p and Au

In the experiment, the cross-section for different processes is measured. However, in order to learn about the quark and gluon distributions, we want to measure the F_2 and F_L structure functions respectively. These can be obtained from the cross-section if we plot the reduced cross-section, σ_r as follows:

$$\sigma_r(x,Q^2) = F_2^A(x,Q^2) - \frac{y^2}{Y^+}F_L^A(x,Q^2)$$

where $Y^+ = 1 + (1-y)^2$. If we plot the reduced cross-section vs y^2/Y^+, for different values of y at the same x,Q^2, it follows that if we fit a straight line to the data, then the intercept on the ordinate gives $F_2^A(x,Q^2)$ and the negative of the slope yields $F_L^A(x,Q^2)$. If there are saturation effects in the gluon distribution, then we would expect these to also manifest themselves in the F_L distribution. Figure 7 shows one such expectation, plotting the fractional contribution to F_L from the higher order (or saturation) terms in the eRHIC x,Q^2 acceptance [5]. On the left, the distribution for protons shows little effect at eRHIC but large effects are predicted for Au nuclei. Figure 8 shows the ratios of F_2(F_L) in nuclei to that in a proton which would be unity in the absence of nuclear effects. The shaded areas show that current theoretical models are currently very poorly constrained by existing data [6],[7]. Also shown on each plot are statistical and systematic uncertainties for running 1 month at 3 different energies. Whilst the systematics are dominant, they show that this measurement will still provide excellent input to the models and help to provide constraints on the partonic composition of nuclei.

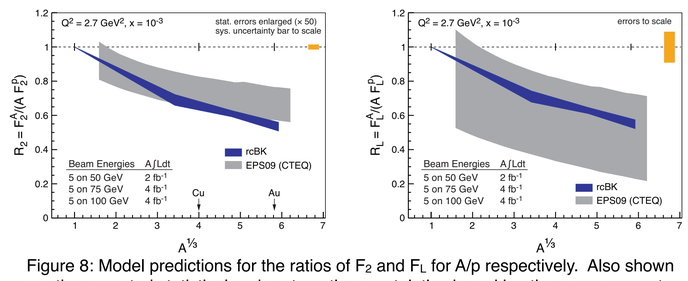

Figure 8: Model predictions for the ratios of F_2 and F_L for A/p respectively. Also shown are the expected statistical and systematic uncertainties in making the measurement

Key Measurements 2: di-hadron Correlations

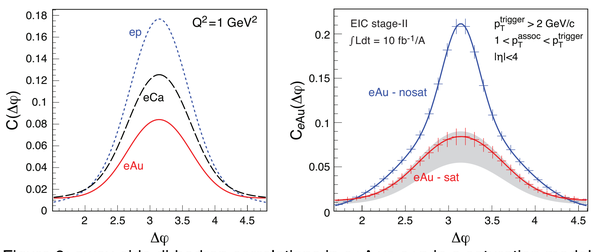

Figure 9: away-side di-hadron correlations in e+A vs e+p in a saturation model together with predicted error bars for 6 months of running at eRHIC

One of the highlights of the RHIC physics programme to date has been the suppression of di-hadron correlations at mid-rapidity in Au+Au collisions,. This measurement was extended to d+Au collisions where no such suppression was observed, one of the key signatures for a de-confined state of matter being produced in the final state at RHIC and is sensitive to not only the gluon distribution, but also gluon correlations at small-x. This was then further explored in correlations of hadrons at forward rapidities where, unlike at mid-rapidity, a suppression of the peak at Δφ = π was observed. This suppression has been shown to be consistent with what would be expected in a CGC model however, one of the difficulties is that the system is not clean and the x,Q^2 of the collision is not known. Therefore, in order to investigate this further, it is important to perform these measurements in *e*+A collisions. Figure 9 (left) shows predictions for di-hadron correlations in *e*+*p*, *e*+Ca and *e*+Au collisions within the framework of a saturation model. The prediction is that there is a suppression of a factor of 2 compared to *e*+*p* collisions. The right side of Figure 9 shows a comparison to a non-saturation model and the statistical uncertainties associated with 6 months running. Also at eRHIC, the J_{eAu} quantity will be explored. This represents the relative yield of back-to-back hadron pairs in *e*+Au collisions compared to *e*+*p*. This ratio was first explored in d+Au collisions at RHIC and shown to be consistent with a saturation model [8]. The left side of Figure 10 shows the expectations for eRHIC in both saturation and non-saturation models together with the expected statistical uncertainties for 6 months running. This will be enough to distinguish between the two scenarios.

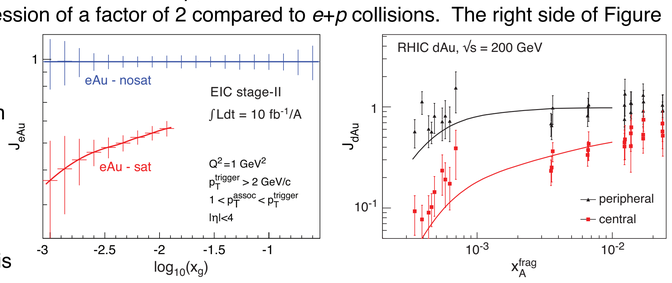

Figure 10: J_{eAu} predictions at eRHIC in a saturation model

Key Measurements 3: Diffraction

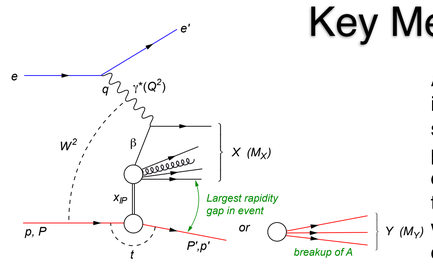

Figure 11: A schematic of a diffractive collision

As well as DIS, diffractive collisions are also of interest. That is, the electron probe interacts with a colour-neutral excitation in the nucleus (often called a Pomeron) as shown in Figure 11. These events are characterised in the experiment by a gap in particle production at forward rapidity. The nucleus can either stay intact (coherent diffraction) or break up (incoherent). The former case is very sensitive to the space-time gluon distribution whilst the latter is sensitive to gluon correlations. At HERA, it was found that diffractive events made up 10-15% of the cross-section and in *e*+Au collisions at eRHIC, it is expected that this will increase to 30-40%. Whilst some aspects of diffraction can be understood in terms of pQCD, not everything can, such as the energy independence of the diffractive-to-total cross-section ratio.

In *e*+*p* collisions, it is possible to differentiate between the two event classes by measuring the proton in a forward spectrometer. This cannot be done in *e*+A collisions, but coherent diffractive events can still be detected via the presence of a rapidity gap and no break-up neutrons in a ZDC. An example of an interesting measurement is that of vector meson production which is extremely clean as there are no other particles in the final state in the detector. Figure 12 shows results from a MC simulation (Sartre event generator) of φ production in *e*+Au collisions as a function of |t|, the momentum transfer at the hadron vertex in Figure 11 passed through an experimental filter. The coherent distribution is reminiscent of a diffractive pattern in optics and the Fourier transform of this distribution can give the spatial distribution of gluons in the nucleus. Statistical uncertainties for both coherent and incoherent diffractive events in 6 months running at eRHIC are depicted in Figure 12 for both saturation and non-saturation models. In the case of the φ, there is a measurable difference and the small error bars would allow for the two scenarios to be distinguished. Note that the incoherent distribution is dominant except at very small |t| but it has been studied that this can be suppressed experimentally by two orders of magnitude, allowing for the first 3 minima in the coherent distribution to be measured.

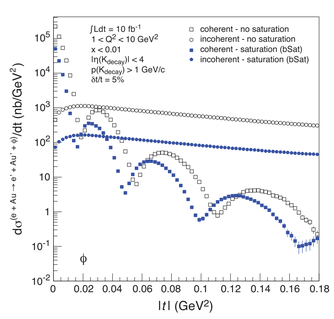

Figure 12: |t| distribution of the φ meson in coherent and incoherent diffractive events

[1] "Gluons and the quark sea at high energies: Distributions, polarization and tomography.", Eds D. Boer, M. Diehl, R. Miler, R. Venugopalan, W. Vogelsang, BNL-96164-2011, INT-PUB-11-034, JLAB-THY-11-1373

[2] HERA structure functions working group, Nucl. Phys. **B181-182** 57-61 (2008)

[3] J. Jalilian-Marian, A. Kovner, A. Leonidov, and H. Weigert, Phys. Rev. **D59**, 014014 (1998)

[4] E. Iancu, A. Leonidov, and L. D. McLerran, Phys. Lett. **B510**, 133 (2001)

[5] J. Bartels, K. Golec-Biernat, and L. Motyka, Phys. Rev. **D81**, 054017 (2010)

[6] J. L. Albacete, N. Armesto, J. G. Milhano, and C. A. Salgado, Phys. Rev. **D80**, 034031 (2009)

[7] K. J. Eskola, H. Paukkunen, and C. A. Salgado, JHEP **04**, 065 (2009)

[8] PHENIX Collaboration, A. Adare et al., Phys.Rev.Lett. **107**, 172301 (2011)

Office of Science
U.S. DEPARTMENT OF ENERGY

BROOKHAVEN NATIONAL LABORATORY